# Evaluation of radon adsorption efficiency values in xenon with activated carbon fibers

Nakano, Y. ; Ichimura, K. ; Ito, H. ; Okada, T. ; Sekiya, H. ; Takeuchi, Y. ; Tasaka, S. ; Yamashita, M.

(Citation)
Progress of Theoretical and Experimental Physics,2020(11):113H01-113H01

(Issue Date)
2020-11

(Resource Type)
journal article

(Version)
Version of Record

PTEP

Prog. Theor. Exp. Phys. **2020**, 113H01 (15 pages)
DOI: 10.1093/ptep/ptaa119

# Evaluation of radon adsorption efficiency values in xenon with activated carbon fibers

Y. Nakano[1], K. Ichimura[2,3], H. Ito[4], T. Okada[4], H. Sekiya[4,3], Y. Takeuchi[1,3,*], S. Tasaka[4], and M. Yamashita[3,4,5]

[1]*Department of Physics, Graduate School of Science, Kobe University, Kobe, Hyogo 657-8501, Japan*
[2]*Research Center for Neutrino Science, Tohoku University, Sendai, Miyagi 980-8578, Japan*
[3]*Kavli Institute for the Physics and Mathematics of the Universe (WPI), The University of Tokyo Institutes for Advanced Study, University of Tokyo, Kashiwa, Chiba 277-8583, Japan*
[4]*Kamioka Observatory, Institute for Cosmic Ray Research, The University of Tokyo, Gifu 506-1205, Japan*
[5]*Present address: Institute for Space-Earth Environmental Research, Nagoya University, Nagoya, Aichi 464-8601, Japan*
*E-mail: takeuchi@phys.sci.kobe-u.ac.jp

Received March 30, 2020; Revised July 22, 2020; Accepted August 4, 2020; Published November 2, 2020

The radioactive noble gas radon-222 ($^{222}$Rn) produced in the uranium series is a crucial background source in many underground experiments. We have estimated the adsorption property of Rn with activated carbon fibers (ACFs) in air, argon, and xenon gas. We evaluated six ACFs, named A-7, A-10, A-15, A-20, A-25, and S-25, provided by Unitika Ltd. We measured the intrinsic radioactivity of these ACF samples, and found A-20's radioactivity of the uranium series to be $< 5.5$ mBq/kg with 90% confidence level. In air and Ar gas, we found that ACF A-15 has an adsorption efficiency of 1/10000 reduction at maximum before saturation of Rn adsorption, and more than 97% adsorption efficiency after the saturation. In Xe gas, we found that ACF A-20 has the best Rn adsorption ability among the tested ACFs. We also found that S-25, A-25, and A-15 have similar Rn adsorption performance.

Subject Index H20

## 1. Introduction

### *1.1. Xenon for underground experiments and radon background*

Xenon is one of the attractive materials in the field of particle physics experiments. Since Xe has no long-lived radioactive isotopes of its own it is intrinsically radio-pure, except for the double beta decay ($^{136}$Xe) and double electron capture ($^{124}$Xe) nuclides [1,2]. Because of its nuclear properties (such as spin and atomic mass number) and its ease of scalability, Xe is widely used as a target of direct dark matter searches [3–6] and a source of double beta decay searches [7–10] in underground experiments. Recently, other decay processes of the Xe atom, such as neutrinoless double electron capture ($0\nu$ECEC) or neutrinoless quadruple beta decay ($0\nu 4\beta^-$), have been proposed to theoretically explain lepton number violation [11–13].

In these rare event search experiments, radioactive impurities in liquid or gas Xe are severe background sources. In particular, the noble gas radon-222 ($^{222}$Rn) is continuously produced from the decay of radium-226 ($^{226}$Ra) in the detector material. Because of its long decay time (about 3.8 days), the Rn produced enters the sensitive volume of the detector and results in the generation of mimic signals below the multi-MeV region. Therefore, the removal of Rn in Xe is an essential technique to improve the sensitivity of such experiments [14,15].

**Table 1.** Summary of basic properties of ACFs provided by Unitika Ltd (information provided by Unitika). Meso pore volume ratio is the ratio of the pore volume of meso pores (2–50 nm) to the whole pore volume of an ACF.

| | A-7 | A-10 | A-15 | A-20 | A-25 | S-25 |
|---|---|---|---|---|---|---|
| Specific surface area [$m^2/g$] | 850 | 1300 | 1700 | 2000 | 2667 | 1744 |
| Average pore diameter [nm] | 1.7 | 1.7 | 1.9 | 2.2 | 2.5 | 5.3 |
| Pore volume [$cm^3/g$] | 0.35 | 0.55 | 0.80 | 1.11 | 1.65 | 2.30 |
| Meso pore volume ratio [%] | 4 | 6 | 10 | 21 | 37 | 67 |

There are two strategies to reduce Rn in the detector: one is careful material screening before detector construction, and the other is Rn removal during the observation phase with the detector. Before constructing the detector, the radio impurity of the materials should be measured with a screening device such as a high-purity germanium detector, inductively coupled plasma mass spectrometry (ICP-MS), or any other special screening systems [16–22].

Once the detector is constructed, the Rn emanation from any type of material is basically fixed. Therefore, emanating Rn should be removed through a purification process. Several studies of Rn removal in Xe gas have been conducted, for example the development of a distillation column and single-column adsorption using activated charcoal [23–25]. Both Rn removal techniques have merits and demerits. In the case of adsorption, separation of Xe and Rn using an adsorbent is challenging because both elements are noble gases and have similar molecule sizes. Therefore, it is important to use an appropriate adsorbent for the selective adsorption of Rn in Xe.

### *1.2. Activated carbon fiber*

Activated charcoal is an effective adsorbent for various impurities by a physical process based on van der Waals forces and the polarizability of the atoms [26]. For example, activated charcoal has an excellent ability to remove Rn from argon [27]. However, when the molecule sizes of the inert gas and Rn are similar, such as Xe, both Rn and Xe tend to be adsorbed by the adsorbent. Therefore, the average pore size of the adsorbent should be selected carefully. Another valuable property is the effective surface area of the adsorbent. Larger surface areas allow increased adsorption efficiency. Furthermore, since Rn emanation from the adsorbent itself ultimately limits the Rn removal ability, it is necessary to reduce the amount of internal radioactive impurities in the adsorbent.

Activated carbon fiber (ACF) has been commercially available since the 1990s [28]. It is a major adsorbent because it has a large surface area and good adsorption properties. The general adsorption properties of ACF have been reported in various papers [29–32]. However, its application to adsorbing Rn in Xe gas has not yet been reported.

For this study, several kinds of ACFs were specially provided by Unitika Ltd.[1] Figure 1 shows a picture of a typical ACF provided by Unitika Ltd.

The ACFs provided are named A-7, A-10, A-15, A-20, A-25, and S-25. Among them, A-25 and S-25 are test products, and the others are commercial products. For selective Rn adsorption, the pore parameters are essential. Such basic properties of these ACFs are summarized in Table 1.

The purpose of this report is to provide the basic Rn adsorption performance of these ACFs in Xe in various conditions. It consists of five sections, including this introduction. In Sect. 2 we describe the

[1] https://www.unitika.co.jp/e/index.html.

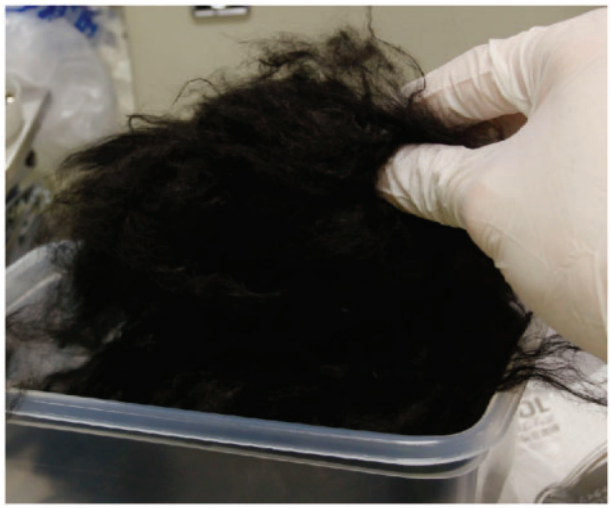

**Fig. 1.** A typical ACF provided by Unitika Ltd.

radioactive impurities of those ACFs and compare their radioactivity with other activated charcoals reported in earlier studies. In Sect. 3 we describe the measurement system designed to evaluate the Rn adsorption efficiency of the ACFs. Then, we present the performance of this system using purified air, Ar gas, and Xe gas. In Sect. 4 we present the characteristic dependence of Rn adsorption in Xe, and show comparisons of the adsorption efficiency among the ACFs. The last section summarizes the study.

## 2. Radioactive impurity measurements

As explained in Sect. 1, the radon emanation from an adsorbent limits the Rn adsorption ability. Therefore, low intrinsic radioactivity of $^{226}$Ra (or uranium series) is required for an adsorbent. We measured the intrinsic radioactive contamination of the provided ACFs with high-purity germanium detectors (HPGe) at Kamioka Observatory, the Institute for Cosmic Ray Research (ICRR), the University of Tokyo, and at Kavli Institute for the Physics and Mathematics of the Universe (IPMU), the University of Tokyo. For this evaluation we measured four ACFs, A-10, A-15, A-20, and A-25. We put them into an EVOH (ethylene-vinylalcohol copolymer) plastic bag in order to keep emanated Rn from the samples; then, measurements were carried out for about 10 days after reaching radiation equilibrium. This HPGe assay method is reported in Ref. [33].

The results of the measurements are summarized in Table 2, along with other measurements of activated charcoals by the XMASS collaboration [25] and the XENON collaboration [34].

For these ACFs, we could not observe any significant gamma-ray line over the background spectrum in the measurements in Table 2.[2] Therefore, we have estimated the upper limits. The obtained upper limit of A-20 is $< 5.5$ mBq/kg for the uranium series. Comparing the radioactivity of the uranium series with other reports [25,34], A-20 has a lower radioactivity than Shirasagi $G_{2X}$ 4/6. However, we could not judge whether A-20 has a lower (or higher) radioactivity than Blücher 100050.[3]

[2] However, we observed $63 \pm 9$ mBq/kg of $^{228}$Th (half-life 1.9 years) only in the A-20 sample. We think this was contamination in the preparation process of this A-20 sample, and that this contamination would not affect $^{222}$Rn assays.

[3] There is a difference in the estimation. A PC measures emanated radon from the sample only, but an HPGe detector also measures radioisotopes inside the sample.

**Table 2.** Summary of intrinsic radioactivities of A-10, A-15, A-20, and A-25. Measurements of activated charcoals are also shown. The measurement device is a high-purity germanium detector (HPGe) or proportional counter (PC). For the HPGe measurements, lead-214 ($^{214}$Pb) and bismuth-214 ($^{214}$Bi) were used for the estimation of the uranium series, and actinium-228 ($^{228}$Ac) for the estimation of the thorium series. The upper limit values are 90% confidence level.

| | Method | Weight [g] | Duration [day] | Uranium series [mBq/kg] | Thorium series [mBq/kg] | $^{40}$K [mBq/kg] |
|---|---|---|---|---|---|---|
| A-10 | HPGe | 6.65 | 12.4 | $< 352$ | $< 305$ | $< 4.31 \times 10^3$ |
| A-15 | HPGe | 160.0 | 10.1 | $< 11.9$ | $< 12.2$ | $< 142$ |
| A-20 | HPGe | 267.4 | 11.6 | $< 5.5$ | $< 10.4$ | $< 49$ |
| A-25 | HPGe | 8.4 | 14.9 | $< 269$ | $< 261$ | $< 4.31 \times 10^3$ |
| Shirasagi $G_{2X}$ 4/6 [25] | HPGe | 95.0 | 7.0 | $67 \pm 15$ | — | — |
| Shirasagi $G_{2X}$ 4/6 [34] | PC | — | — | $62 \pm 4$ | — | — |
| Blücher 100050 [34] | PC | — | — | $2.6 \pm 0.3$ | — | — |

## 3. Experimental setup

### *3.1. Test measurements with purified air and argon*

As a first step, we evaluated the Rn adsorption performance of ACF in purified air and in purified Ar. We used G1-grade purified gases (impurities less than 0.3 ppm) provided by the Taiyo Nippon Sanso Corporation [35]. Since the molecular sizes of nitrogen, oxygen, and Ar are relatively small compared with that of Rn, the adsorption of Rn in purified air or Ar is expected to be efficient. To date, adsorption techniques of Rn in air or $N_2$ with activated charcoals have been established among underground experiments [36–40].

In order to perform the test measurements with air or Ar, we constructed a test bench at Kobe University, Japan. The test bench is based on the measurement system developed in Ref. [27]. The test bench for this study consists of a high-sensitivity 80-L Rn detector [36,41], a gas mass flow controller (Horiba STEC, SEC-Z512MGX, hereafter MFC), a gas circulation pump (Enomoto Micro Pump Mfg. Co. Ltd, MX-808ST-S), a dew point gauge (Vaisala, DMT152), a pressure gauge (Swagelok, PGU-50-MC01-L-4FSF), filters (Nippon Seisen Co. Ltd, NASclean GF-T001 and GF-D03N), a refrigerator with a cold trap, and a Rn source (Pylon, RNC). The radioactivity of this source was 78.3 Bq ($^{226}$Ra). The refrigerator is equipped with a box-shaped cold trap [27]. A schematic view of this test bench is shown in Fig. 3 in Sect. 3.2, though without the main trap in that figure.

The principal techniques of the 80-L Rn detector are the electrostatic collection of the positively charged daughter nuclei of $^{222}$Rn [42,43] and the deposit energy measurement of their $\alpha$ decays on a PIN photodiode [36,41,44–47]. The 80-L Rn detector can measure a few mBq/m$^3$ level of Rn concentration in the circulation gas. Details of the 80-L Rn detector can be found in Refs. [36,41].

Here are the typical operations before the test measurements with this test bench. For the measurements in this section, we put 4.75 g of ACF A-15 into the box-shaped trap. Then, we baked the trap at $+85$°C under vacuum with a turbo molecular pump. After the vacuum pressure became less than $1.0 \times 10^{-1}$ Pa we stopped the baking, then started cooling down the box-shaped trap to $-105$°C. In parallel, the test bench was filled with purified air or Ar. When we changed the gas in the system, the entire system was evacuated before filling, except for the Rn source. The Rn source was purged with the new gas in advance. The typical pressure of the gas in the system was atmospheric pressure (around 0.10 MPa in absolute pressure, or $\pm 0.000$ MPa in gauge pressure). Note that in this report

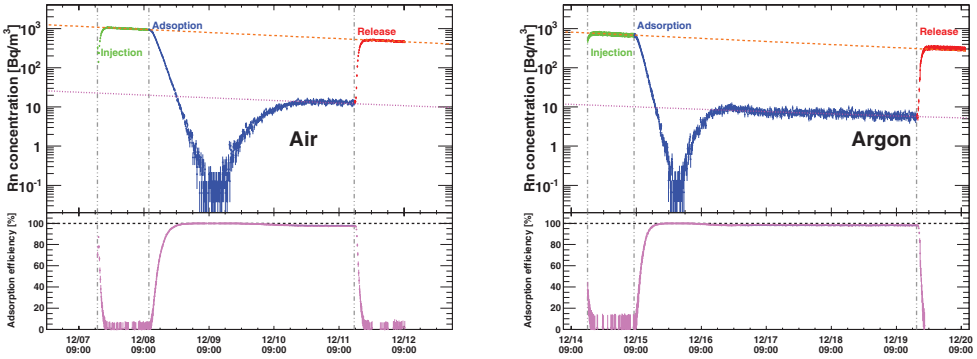


**Fig. 2.** The left (right) plot shows measurements with purified air (Ar). The upper (lower) panel shows the Rn concentration (Rn adsorption efficiency) as a function of time. In the top panel, the colored data points show the different phases of the measurements, where green, blue, and red show the Rn concentration in the injection phase, the adsorption phase, and the release phase, respectively. The orange (pink) line in the upper panel shows the Rn decay curve for expected (remaining) Rn concentrations.

we use gauge pressure values to express the inner gas pressure of the test bench if not otherwise specified. The gas was circulated with the circulation pump after filling.

There were three steps after the preparation of the cold trap and the circulation gas. The first phase was injection of Rn into the circulation gas from the Rn source. The second phase was adsorption of Rn with the cooled box-shaped trap. The third phase was the release of Rn from the trap by heating the trap to the normal temperature (between $+15°$C and $+25°$C). During these phases, the flow rate of the circulation gas was kept the same using the MFC. The 80-L Rn detector was also continuously monitoring the Rn concentration in the circulation gas during these phases. The observed number of polonium-214 ($^{214}$Po) events from the 80-L Rn detector was summarized every 10 minutes, and the observed count rate converted into the Rn concentration with the calibration factor in Refs. [36,41]. Therefore, we obtained the Rn concentration in the circulation gas every 10 minutes.

Figure 2 shows the results of these test measurements. For the test measurement with air, we injected Rn at 15:51 on December 7, 2016. The gas circulation rate was 0.90 SLM (liters per minute at standard temperature and pressure), and then we started the adsorption phase from 10:52 on December 8. The Rn concentration dropped soon after starting the adsorption phase and it took about 24 hours to reach the lowest value. At this moment, the Rn adsorption efficiency reached a maximum of nearly 100% with a reduction factor of $10^4$.

In general, further adsorption is not expected when all pore sites are filled with gas molecules. In such a situation, adsorbed Rn is eventually released from the ACF by collision with other molecules in the circulation gas. Consequently, some of the Rn returns to the circulation gas again because of such saturation. This situation is called break-through. The Rn concentration in the system ultimately reaches an equilibrium state between adsorption and release.

In the measurements with air or Ar, the Rn concentration gradually increased to $\sim$10 Bq/m$^3$ after reaching the lowest value, and this is explained above. During this phase, the Rn adsorption efficiency finally becomes $97.9 \pm 0.1\%$. After starting the release phase at 14:39 on December 11, the Rn concentration immediately increased and then reached the originally expected level.

For the test measurement with Ar, we evaluated the Rn adsorption efficiency with the same procedure and a gas circulation rate of 1.3 SLM. The result is shown in Fig. 2 (right). The Rn adsorption

**Table 3.** Summary of the Rn adsorption efficiency in purified air and Ar with A-15. The definition of the Rn adsorption efficiency is explained in Sect. 3.4. The possible systematic uncertainties are pressure drop in the adsorption phase (−2.0%), accuracy of the pressure (−1.0%), and reproducibility (±2.0%).

| Gas | Flow rate [SLM] | Rn adsorption efficiency [%] |
|---|---|---|
| Air | 0.90 | $97.9 \pm 0.1$ (stat.) |
| Argon | 1.3 | $98.3 \pm 0.1$ (stat.) |

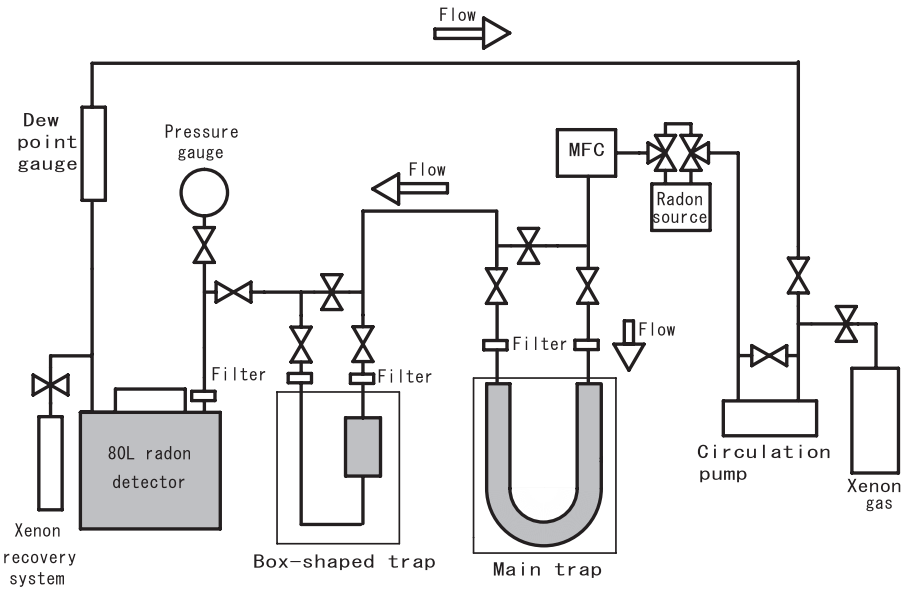


**Fig. 3.** Experimental setup of the full test bench. The Rn detector was upgraded to an 80-L detector from the system in Ref. [27]. Then, a new refrigerator and a new larger cold trap (main trap) were newly added for the measurements with Xe gas. The arrows show the direction of the circulation gas flow.

efficiency is determined to be $98.3 \pm 0.1\%$, as summarized in Table 3. Though the adsorption efficiencies of air and Ar are similar, the break-through time of Ar looks shorter than that of air. This would be due to the difference in the gas flow rates of these tests. From these test measurements, we demonstrated that this system can precisely measure the Rn adsorption efficiency of ACF in both air and Ar. In addition to this, we found that ACF A-15 showed good Rn adsorption efficiency.

### *3.2. Measurement system for Xe gas*

For the measurements using Xe gas, we added a new refrigerator with a larger cold trap to increase the amount of the ACF sample. A schematic diagram of the full system is shown in Fig. 3. The gas in the system was circulated by the circulation pump. The Rn concentration in the circulation gas was measured with the 80-L Rn detector. The pressure, temperature, and dew point were monitored continuously during the measurement.

In this system, two cold traps (main trap and box-shaped trap) were used. The main trap is a U-shaped electro-polished stainless steel pipe, and can typically hold 10–20 g of an ACF sample. The main trap is used to hold the ACF sample to estimate Rn adsorption efficiency, and its volume is 122 $cm^3$. The temperature of the ACF sample was controlled by the refrigerator for the main trap. Photographs of the main trap are shown in Fig. 4. The box-shaped trap is used to control the humidity in the circulation gas for the measurements with Xe. In the actual measurement with Xe gas, the

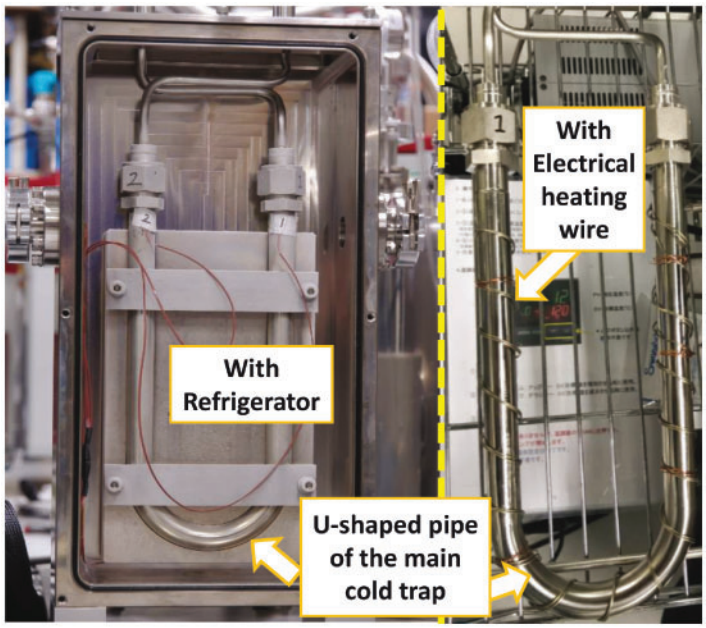


**Fig. 4.** Photographs of the main trap. The left side shows the trap in the cooling system for the adsorption phase, and the right side shows the trap with an electrical heating wire for baking in the release phase.

box-shaped trap was always kept at $-70$°C to maintain low humidity conditions. We tested this box-shaped trap in Xe gas, then confirmed that the effect from the box-shaped trap was negligible in Xe gas.

In order to prevent possible contamination of carbon fibers from the ACF sample in the measurement system, thin-layer metal membrane filters (0.0025 $\mu$m and 0.3 $\mu$m) were installed at the inlet and outlet of the cold traps.

### *3.3. Measurement method*

Here is the typical measurement method with the main trap. Before the measurements, we put an ACF sample into the main trap. Then we evacuated the main trap, baking it at $+180$°C. After the vacuum pressure became less than $1.0 \times 10^{-1}$ Pa in absolute pressure we stopped the baking, and then put the main trap into the cooling system. Finally, the measurement system was filled with Xe gas. The typical circulation gas pressure was at atmospheric pressure, but it was reduced down to $-0.071$ MPa in the case of the pressure dependence measurement described in Sect. 4.3. The Xe gas was circulated with the pump after filling at 0.14–1.4 SLM.

The three steps (injection, adsorption, and release phases) are the same as described in Sect. 3.1, but the temperature condition was changed for the main trap. All the temperature settings of the main refrigerator during the adsorption phase were $-95$°C. The typical temperature setting during the release phase was normal temperature. In some measurements, the temperature at the beginning of the release phase was set at $+180$°C to increase the release speed. In each step, the measurement continued until the count rate of the Rn detector became stable. The adsorption phase was started by switching the inlet and outlet valves of the main trap from bypass mode to through-trap mode. Using the 80-L Rn detector, the Rn concentration in the circulation gas was continuously monitored.

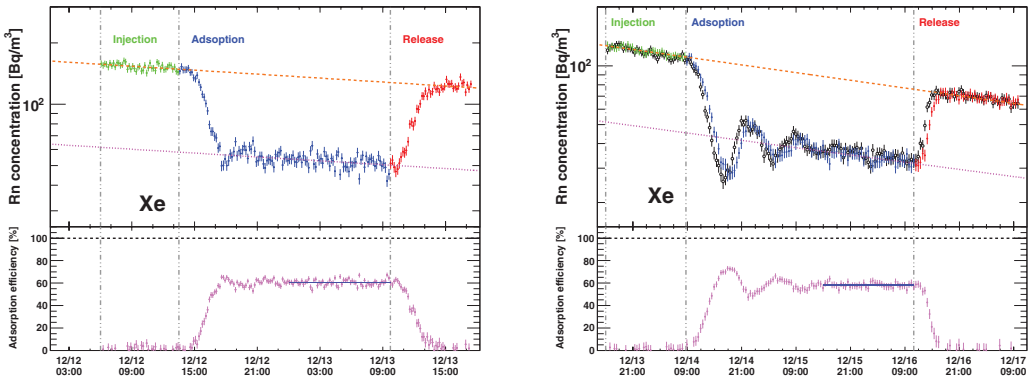


**Fig. 5.** An example of the measurements with Xe gas with ACF A-25. The Xe gas pressure before the adsorption phase, Xe gas pressure before the release phase, and flow rate in left (right) are −0.071 MPa (−0.071 MPa), −0.076 MPa (−0.075 MPa), and 0.41 SLM (0.14 SLM), respectively. The plot and color definitions are the same as Fig. 2. The black open circles in the upper right plot are the Rn concentration obtained from $^{218}$Po counts.

### *3.4. Data analysis*

In order to measure the Rn adsorption efficiency in the circulation gas, we performed the following analysis procedure. At first, the Rn concentration in the circulation gas was determined by fitting with the Rn decay curve, defined as $C_0 e^{-\lambda t} + C_1$ [Bq/m$^3$], where λ is the decay constant of $^{222}$Rn, $t$ is elapsed time, and $C_0$ and $C_1$ are parameters to be fitted. Applying this equation to the data before the adsorption phase, the expected Rn concentration without Rn adsorption ($C_{\text{expected}}$) at $t = 0$ is obtained as $C_0 + C_1$ [Bq/m$^3$]. When this equation is applied to the data during the adsorption phase, the remaining Rn concentration after Rn adsorption by the cold trap ($C_{\text{remaining}}$) at $t = 0$ is also obtained. The expected fitted line is compared with the data after the release phase, in order to check the consistency of the $C_{\text{expected}}$ value.

Then, we compare the remaining Rn concentration with the expected Rn concentration as follows:

$$R = \frac{C_{\text{expected}} - C_{\text{remaining}}}{C_{\text{expected}}} \times 100.0\ [\%]. \tag{1}$$

In this report, we use $R$ [%] as the Rn adsorption efficiency.

### *3.5. A typical measurement in Xe gas and systematic uncertainty*

Figure 5 shows an example of the measurements with Xe gas. In these measurements, ACF A-25 was used in Xe circulation gas at −0.071 MPa, and we observed a clear drop of the Rn concentration during the adsorption phase. The Rn concentration drops in 0.41 SLM and 0.14 SLM flow rate measurements are very similar at around 60%. An apparent oscillation of the Rn concentration in the adsorption phase is observed in the 0.14 SLM flow rate measurement. This behavior is similar to Ref. [25].

We also observed a pressure difference between the adsorption phase and other phases. The pressure drop during the adsorption phase was due to the adsorption of both Xe and Rn by the ACF. This pressure difference suggests that the actual Rn adsorption efficiency might be lower than the observed $R$ defined in Sect. 3.4. Therefore, we have evaluated the amount of the pressure difference as a systematic uncertainty on the Rn adsorption efficiency.

In the case of the 0.41 SLM measurement, the pressure difference was 0.0050 MPa and the absolute pressure before the adsorption phase was 0.0303 MPa. Based on this difference, we assigned a

**Table 4.** Summary of the systematic uncertainties on the Rn adsorption efficiency.

| Source | Uncertainty |
|---|---|
| Pressure drop in adsorption phase | −5.0% (typical) |
| Accuracy of pressure | Between −3.0% (at −0.07 MPa) and −1.0% (at 0.00 MPa) |
| Reproducibility | ±2.0% |

systematic error of −16.5% on the absorption efficiency. Typical gauge pressure values of the circulation gas were ±0.000 MPa in the adsorption phase and +0.005 MPa in other phases, except for the pressure dependence measurement. This pressure difference corresponds to −5.0% systematic uncertainty, typically.

The accuracy of the pressure of the circulation gas has around ±0.001 MPa uncertainty, since the pressure gauge is an analog type. Because of this accuracy, we assigned a few % level of uncertainty on the Rn adsorption efficiency. This systematic uncertainty ranges from −3.0% to −1.0% depending on the pressure inside the system (−3.0% for the lowest case of −0.07 MPa and −1.0% for atmospheric pressure). This uncertainty will reduce or enhance the uncertainty on the Rn adsorption efficiency from the pressure drop. We estimated maximum enhancement as a systematic error source.

In measurements under very similar conditions, the observed Rn adsorption efficiency was slightly different within a few %. Therefore, we assigned the systematic uncertainty from reproducibility as ±2.0%. The assigned systematic uncertainties in this study are summarized in Table 4.

The observed Rn adsorption efficiency values in Xe of the 0.41 SLM and 0.14 SLM flow rate measurements were $60.8 \pm 0.3(\text{stat.})^{+2.0}_{-16.9}(\text{syst.})\%$ and $58.5 \pm 0.3(\text{stat.})^{+2.0}_{-13.6}(\text{syst.})\%$, respectively. The uncertainty from the pressure drop in the adsorption phase is estimated with the actual pressure drop in each measurement.

In preceding studies [25,34], the velocity ratio (or retention time ratio) of Rn to Xe in the adsorbent was estimated as the Rn trap performance of the test system. We also estimated the velocity ratio from the measurement in Fig. 5 (right). In this measurement, we observed the retention time of Rn ($T_{\text{Rn}}$ in Ref. [25]) in the main trap as $10 \pm 2$ hours, using the $^{218}$Po data; then, the velocity ratio becomes $v_{\text{Rn}}/v_{\text{Xe}} = (1.4 \pm 0.2) \times 10^{-3}$ (at −95°C). The corresponding ratios in the preceding studies were $v_{\text{Rn}}/v_{\text{Xe}} = (0.96 \pm 0.10) \times 10^{-3}$ (at −85°C) [25] and $v_{\text{Rn}}/v_{\text{Xe}} = (0.65 \pm 0.11) \times 10^{-3}$ (at −70°C) [34]. This means that the velocity of Rn in the adsorbent column in our test bench (= main trap) was faster than the others. The main reason for this difference would be due to the difference in the density of the adsorbent in the column. From the information in Ref. [25], the adsorbent density in the column was estimated as about 358 kg/m$^3$. On the other hand, for our system it is 98 kg/m$^3$, since we could not pack fibers into the U-shaped column very efficiently.

Then, using this velocity ratio, we also estimate the two-component Henry's constant of the adsorbent $\tilde{H}$ which was introduced in Ref. [34]. They obtained $\tilde{H} = (1.94 \pm 0.24) \times 10^{-3}$ mol/(Pa kg) (at −70°C, −0.080 MPa Xe). From our measurement, we obtained $\tilde{H} = (5.0 \pm 1.0) \times 10^{-3}$ mol/(Pa kg) (at −95°C, −0.071 MPa Xe). Though the conditions of the measurements are different, our adsorbent shows adsorption performance comparable with the preceding work.

**Table 5.** Summary of the flow rate dependence of the adsorption efficiency with A-25.

| Flow rate [SLM] | Rn adsorption efficiency [%] |
|---|---|
| 0.14 | $27.8 \pm 0.2(\text{stat.})^{+2.0}_{-5.5}(\text{syst.})$ |
| 1.4 | $27.4 \pm 0.4(\text{stat.})^{+2.0}_{-5.5}(\text{syst.})$ |

## 4. Result

In this section we describe the measurement results of the Rn adsorption efficiency in Xe gas. As a first step, we evaluated the possible flow rate dependence of the Rn adsorption efficiency using ACF A-25. Then, its Rn concentration dependence and circulation gas pressure dependence was evaluated with A-25. After presenting the results from these dependence measurements, we discuss the Rn adsorption efficiency among the six ACFs provided by the company.

### *4.1. Flow rate dependence*

At first, we evaluated the flow rate dependence of the Rn adsorption efficiency using 10.50 g of A-25. The experimental procedure was the same as the typical measurement explained in Sect. 3.3, but we changed the circulation gas flow rate using the MFC. We also kept the Rn source connected during this measurement in order to maintain the same Rn concentration level. Therefore, the difference should only be the flow rate of the circulation gas. Typical Rn concentration and circulation gas pressure are $10^3$ Bq/m$^3$ and atmospheric pressure, respectively.

The results obtained are summarized in Table 5. Here, the systematic errors are obtained from Table 4. However, for the relative comparison in this estimation, the relevant systematic uncertainty would only be reproducibility (±2.0%), since the pressure drops are very similar in these measurements.

Among these different flow rate measurements, no significant difference was observed. Therefore, we found no significant flow rate dependence of measured Rn adsorption efficiency in the test bench in between 0.14 and 1.4 SLM flow rate.

### *4.2. Rn concentration dependence*

As explained in Sect. 3.1, further adsorption is not expected when all pore sites are filled with gas molecules. Therefore, the Rn adsorption efficiency may depend on the Rn concentration of the circulation gas. In order to evaluate this dependence, we measured the Rn adsorption efficiency under the different Rn concentrations in the circulation gas. In these measurements, 10.50 g of A-25 was used. Typical flow rate and circulation gas pressure were 1.4 SLM and atmospheric pressure, respectively.

Figure 6 shows the measurement results. From Fig. 6 (right), the absorbed Rn amount looks generally proportional to the Rn concentration. Since the Rn concentration corresponds to the partial pressure of Rn gas, this measurement may indicate Henry's law in Rn adsorption [34].

However, from Fig. 6 (left), the Rn adsorption efficiency looks to be increasing in the region below 50 Bq/m$^3$. This dependence suggests that a high Rn absorption efficiency is expected in the real experiments which search for rare physics events, because the Rn concentration level in such experiments is much less than this Rn concentration level. In the region of 50–300 Bq/m$^3$, the Rn concentration dependence of the Rn adsorption efficiency is about ±3%, and this is similar to or slightly smaller than the systematic uncertainty of the Rn adsorption efficiency estimated in Sect. 3.5.

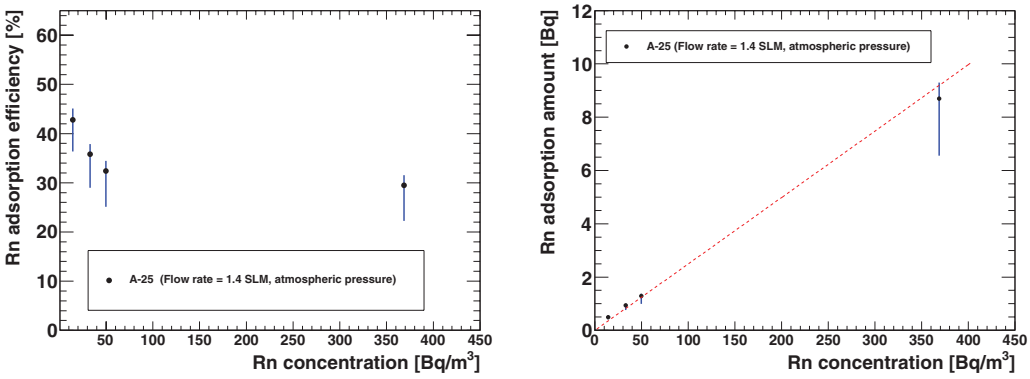


**Fig. 6.** The left (right) plot shows Rn adsorption efficiency (Rn adsorption amount) as a function of the Rn concentration just before the adsorption phase. The black points are observed $R$, and the blue bars are statistical and systematical errors, added in quadrature. The red dashed line on the right is the fit with the straight line (Rn adsorption amount) $=$ $(0.025 \pm 0.001) \times$ (Rn concentration). We used 10.50 g of A-25 in these measurements. The circulation gas pressure of all the data points was atmospheric pressure. The flow rate of the circulation gas was fixed at 1.4 SLM. The temperature setting of the main refrigerator during the adsorption phase was fixed at $-95$°C.

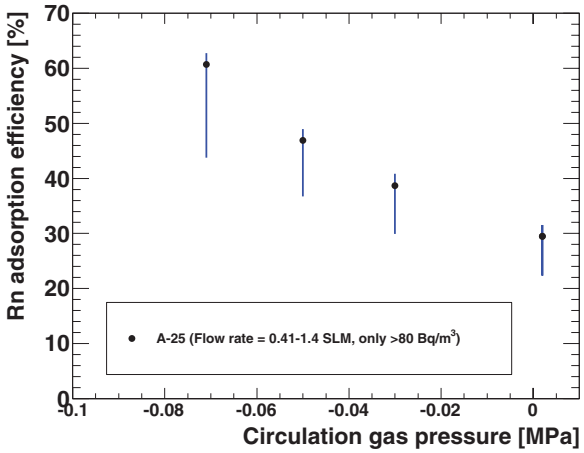


**Fig. 7.** Rn adsorption efficiency as a function of circulation gas pressure. The black points are observed $R$, and the blue bars are statistical and systematical errors, added in quadrature. 10.50 g of A-25 was used. The Rn concentrations of all the data points are above 80 Bq/m$^3$. The flow rate was 1.4 SLM for the atmospheric pressure measurement and 0.41 SLM for the others. The temperature setting of the main refrigerator during the adsorption phase was fixed at $-95$°C.

### *4.3. Pressure dependence*

In general, adsorption depends on both the temperature and the amount of the adsorbed gas molecules. Therefore, the adsorption may depend on the circulation gas pressure inside the system. In order to evaluate the dependence on the circulation gas pressure, we measured the Rn adsorption efficiency of A-25 under different circulation gas pressure. For this measurement, we decreased the circulation gas pressure to $-0.071$ MPa at first. Then, we added Xe gas (with some amount of Rn) into the system to increase the inner gas pressure. Figure 7 shows the results of these measurements. In this estimation, only the data points in which the Rn concentration was more than 80 Bq/m$^3$ were selected to reduce the Rn concentration dependence of the Rn adsorption efficiency.

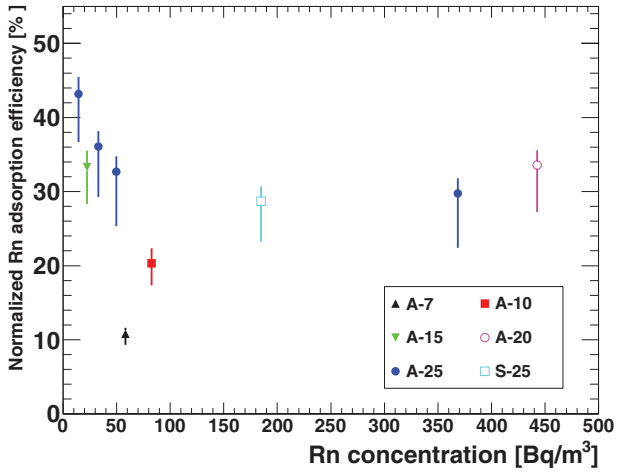


**Fig. 8.** Normalized Rn adsorption efficiency as a function of Rn concentration just before the adsorption phase. The circulation gas pressure was atmospheric pressure, and the flow rate was between 0.14 SLM and 1.4 SLM. The temperature setting of the main refrigerator during the adsorption phase was fixed at −95°C.

We found an apparent increase in the Rn adsorption efficiency when the circulation gas pressure is low.

### *4.4. Comparison among ACF types*

We compared the Rn adsorption efficiency among different ACF types. In this comparison, the measurement data were selected as follows. The circulation gas pressure was atmospheric pressure for all the data, to eliminate pressure dependence of the Rn adsorption efficiency. The flow rate was between 0.14 SLM and 1.4 SLM, where no dependence on the Rn adsorption efficiency was observed. In this comparison we normalized the Rn adsorption efficiency values by weight, to the typical weight of the ACF sample in the main trap (= 12 g), since the amounts of the ACF samples were different. We could not adjust the Rn concentration level in each measurement, though we observed the Rn concentration dependence in the region below 50 Bq/m$^3$. Therefore, this comparison was done as a function of the Rn concentration.

Figure 8 shows a summary of this comparison. Several A-25 measurements are shown as a reference in different Rn concentration regions. Table 6 summarizes the numerical information for typical data points shown in Fig. 8. In Fig. 9, the same measurements are shown using the normalized Rn adsorption amount. In these comparison plots, the dominant uncertainty is the pressure drop effect in the lower error bars. Since it comes from the interpretation of the pressure drop phenomenon, the uncertainties are taken into account among all data points. Therefore, the relative uncertainties among data points would be about twice as large as the upper error bars.

Then, comparing each ACF type to A-25 in a similar Rn concentration area, the normalized Rn adsorption efficiency (and amount) of A-7 and A-10 are lower than that of A-25. On the other hand, A-15, A-20, and S-25 show similar efficiency (and amount) values to A-25. Among these measurements, A-20 shows a slightly higher efficiency (and amount) value than A-25, though they are consistent within the uncertainty. The observed efficiency value of A-20 was $(33.6^{+2.1}_{-6.4})$% (12 g of A-20 in atmospheric pressure Xe and 442.8 ± 0.8 Bq/m$^3$ Rn).

Among A-7, A-10, A-15, and A-20, the adsorption performance looks increasing in this order. From Table 1, the specific surface area, pore volume, and meso pore volume ratio are also increasing

**Table 6.** Summary of the numerical information for typical measurements. The columns, from the left, correspond to ACF type, amount of ACF sample used in the main trap, Rn concentration just before the adsorption phase, pressure drop during the adsorption phase, observed Rn adsorption efficiency $R$, and weight-normalized Rn adsorption efficiency. The errors are statistical only if it is not specified.

| Type | Amount [g] | Rn [Bq/m$^3$] | P. drop [MPa] | $R$ [%] | Normalized efficiency [%] |
|---|---|---|---|---|---|
| A-7 | 29.97 | $58.1 \pm 0.9$ | 0.003 | $27.0 \pm 0.4$ | $10.8^{+0.8}_{-1.5}$(stat.+syst.) |
| A-10 | 12.22 | $82.5 \pm 0.5$ | 0.002 | $20.7 \pm 0.5$ | $20.3^{+2.1}_{-3.0}$(stat.+syst.) |
| A-15 | 11.11 | $22.4 \pm 0.5$ | 0.004 | $30.8 \pm 0.6$ | $33.3^{+2.3}_{-5.0}$(stat.+syst.) |
| A-20 | 12.01 | $442.8 \pm 0.8$ | 0.006 | $33.6 \pm 0.2$ | $33.6^{+2.1}_{-6.4}$(stat.+syst.) |
| A-25 | 11.90 | $368.7 \pm 1.2$ | 0.007 | $29.5 \pm 0.3$ | $29.7^{+2.1}_{-7.4}$(stat.+syst.) |
| A-25 | 11.90 | $14.3 \pm 0.2$ | 0.006 | $42.8 \pm 1.1$ | $43.2^{+2.4}_{-6.5}$(stat.+syst.) |
| S-25 | 11.88 | $184.0 \pm 0.6$ | 0.005 | $28.4 \pm 0.3$ | $28.7^{+2.1}_{-5.5}$(stat.+syst.) |

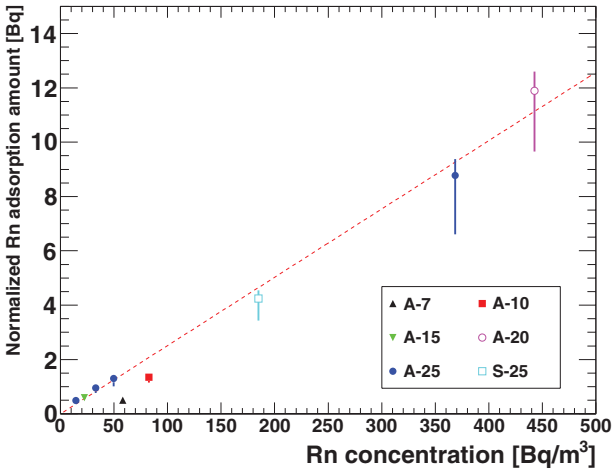


**Fig. 9.** Normalized Rn adsorption amount as a function of Rn concentration just before the adsorption phase. The red dashed line is a fitted line of A-25 data. The measurements used are the same as in Fig. 8

in the same order. Since the kinetic diameters (the Lennard-Jones parameter $\sigma$) of air, Ar, Xe, and Rn gas molecules are estimated as 0.352–0.369 nm, 0.340–0.346 nm, 0.392–0.410 nm, and 0.417–0.421 nm, respectively [48–50], and the typical range of van der Waals interactions is about 1 nm, the relevant pore size on the adsorption would be around 1–2 nm. Therefore, the meso pores (2–50 nm) would not directly affect the adsorption process, while the increase of specific surface area and pore volume would be effective in this comparison.

For A-25 and S-25, the specific surface area and pore volume are larger than A-20, but the measured adsorption performance looks not to be improved. A possible reason would be that the average pore diameter is too large to adsorb Xe atoms, since the intensity of the van der Waals force is inversely proportional to the cube of distance.

## 5. Conclusion

We carried out Rn adsorption measurements with ACFs using a newly developed test bench at Kobe University, Japan. The radioactivity of the ACFs provided by Unitika Ltd was lower than or

comparable to that of the activated charcoals used in previous research. The measured radioactivity of A-20 for the uranium series was $< 5.5\,\mathrm{mBq/kg}$ with a 90% confidence level. In air and Ar gas, ACF A-15 demonstrated an excellent adsorption efficiency of 1/10000 reduction at maximum before saturation of Rn adsorption, and more than 97% adsorption efficiency after saturation. In Xe gas, the adsorption efficiency values were lower than in air or Ar gas. We carried out a set of measurements on Rn adsorption in Xe gas under various conditions, then estimated the ACFs' basic performance in flow rate, concentration, and pressure dependence of Rn adsorption in Xe gas. We also observed some difference in Rn adsorption ability from different ACF types. Among the tested ACFs, A-20 had the best Rn adsorption ability. The observed Rn adsorption efficiency was $(33.6^{+2.1}_{-6.4})\%$ (12 g of A-20 in atmospheric pressure Xe and $442.8 \pm 0.8\,\mathrm{Bq/m^3}$ Rn). S-25, A-25, and A-15 also showed similar adsorption performance.

**Acknowledgements**

The authors are very grateful to Prof. K. Kaneko at Research Initiative for Supra-Materials (RISM), Shinshu University, for his very helpful suggestions on this research topic. The authors also greatly appreciate Unitika Ltd for their kind support of this research. They provided various ACF samples, including some special test products. This work is supported by Japan Society for the Promotion of Science (JSPS) KAKENHI Grant Numbers JP26104008, 18H05536, and 16H03973, and by the joint research program of the Institute for Cosmic Ray Research (ICRR), the University of Tokyo.

## References

[1] A. Gando et al. [KamLAND-Zen Collaboration], Phys. Rev. Lett. **122**, 192501 (2019).
[2] E. Aprile et al. [XENON Collaboration], Nature **568**, 532 (2019).
[3] D. S. Akerib et al., Nucl. Inst. Meth. A **704**, 111 (2013).
[4] E. Aprile et al., Astropart. Phys. **35**, 573 (2012).
[5] K. Abe et al., Nucl. Inst Meth. A **716**, 78 (2013).
[6] X. Cao et al., Sci. China Phys. Mech. Astron. **57**, 1476 (2014).
[7] A. Gando et al. [KamLAND-Zen Collaboration], Phys. Rev. Lett. **117**, 082503 (2016); **117**, 109903 (2016) [erratum].
[8] M. Auger et al., J. Instrum. **7**, P05010 (2012).
[9] P. Ferrario et al. [The NEXT collaboration], J. High Energy Phys. **1601**, 104 (2016).
[10] S. Ban et al., Nucl. Inst. Meth. A **875**, 185 (2017).
[11] J. Barea, J. Kotila, and F. Iachello, Phys. Rev. C **87**, 057301 (2013).
[12] J. Kotil, J. Barea, and F. Iachello, Phys. Rev. C **89**, 064319 (2014).
[13] J. Heeck and W. Rodejohann, Europhys. Lett. **103**, 32001 (2013).
[14] E. Aprile et al., J. Cosmol. Astropart. Phys. **1604**, 027 (2016).
[15] J. Aalbers et al., J. Cosmol. Astropart. Phys. **1611**, 017 (2016).
[16] D. S. Leonard et al., Nucl. Inst Meth. A **591**, 490 (2008).
[17] E. Aprile et al., Astropart. Phys. **35**, 43 (2011).
[18] E. Aprile [XENON Collaboration], Eur. Phys. J. C **77**, 890 (2017).
[19] X. Wang, X. Chen, C. Fu, X. Ji, X. Liu, Y. Mao, H. Wang, S. Wang, P. Xie and T. Zhang, J. Instrum. **11**, T12002 (2016).
[20] S. Cebrián et al., J. Instrum. **12**, T08003 (2017).
[21] K. Abe et al., Nucl. Inst. Meth. A **884**, 157 (2018).
[22] H. Ito, T. Hashimoto, K. Miuchi, K. Kobayashi, Y. Takeuchi, K. D. Nakamur, T. Ikeda, and H. Ishiura, Nucl. Inst. Meth. A **953**, 163050 (2020).
[23] S. Bruenner, D. Cichon, S. Lindemann, T. Marrodán Undagoitia, and H. Simgen, Eur. Phys. J. C **77**, 143 (2017).
[24] E. Aprile et al., Eur. Phys. J. C **77**, 358 (2017).
[25] K. Abe et al., Nucl. Inst. Meth. A **661**, 50 (2012).
[26] S. Maurer, A. Mersmann, and W. Peukert, Chem. Eng. Sci. **56**, 3443 (2001).
[27] M. Ikeda, T. Hokama, S. Tasaka, and Y. Takeuchi, Radioisotopes **59**, 29 (2010).

[28] K. Tai and N. Shindo, Sen'i Gakkaishi **49**, P177 (1993).
[29] K. Kaneko, C. Ishii, M. Ruike, and H. kuwabara, Carbon **30**, 1075 (1992).
[30] M. Aoshima, T. Suzuki, and K. Kaneko, Chem. Phys. Lett. **310**, 1 (1999).
[31] M. Aoshima, K. Fukasawa, and K. Kaneko, J. Coll. Int. Sci. **222**, 179 (2000).
[32] K. Kaneko et al., Chem. Lett. **41**, 466 (2012).
[33] S. Ito, K. Ichimura, Y. Takaku, K. Abe, M. Ikeda, and Y. Kishimoto, Prog. Theor. Exp. Phys. **2018**, 091H01 (2018).
[34] S. Lindemann, PhD thesis, Heidelberg University (2013). (Available at http://archiv.ub.uni-heidelberg.de/volltextserver/15725/, date last accessed August 15, 2020).
[35] Taiyo Nippon Sanso Corporation, *High Purity Gas* (Taiyo Nippon Sanso Corporation, Tokyo, 2020). (Available at: http://www.tn-specialtygases.jp/catalog/pure/, date last accessed August 15, 2020).
[36] Y. Nakano, H. Sekiya, S. Tasaka, Y. Takeuchi, R. A. Wendell, M. Matsubara, and M. Nakahata, Nucl. Inst. Meth. A **867**, 108 (2017).
[37] S. Fukuda et al., Nucl. Inst. Meth. A **501**, 418 (2003).
[38] J. Boger et al. [The SNO Collaboration], Nucl. Inst. Meth. A **449**, 172 (2000).
[39] A. Nachab and the NEMO collaboration, AIP Conf. Proc. **897**, 35 (2007).
[40] G. Zuzel, AIP Conf. Proc. **1921**, 050001 (2018).
[41] K. Hosokawa, A. Murata, Y. Nakano, Y. Onishi, H. Sekiya, Y. Takeuchi, and S. Tasaka, Prog. Theor. Exp. Phys. **2015**, 033H03 (2015).
[42] P. Kotrappa, S. K. Dua, P. C. Gupta, and Y. S. Mayya, Health Phys. **41**, 35 (1981).
[43] P. K. Hopke, Health Phys. **57**, 39 (1989).
[44] M. Nemoto, S. Tasaka, H. Hori, K. Okumura, T. Kajita, and Y. Takeuchi, Radioisotopes **46**, 710 (1997).
[45] Y. Takeuchi, K. Okumura, T. Kajita, S. Tasaka, H. Hori, M. Nemoto, and H. Okazawa, Nucl. Inst. Meth. A **421**, 334 (1999).
[46] J. Kiko, Nucl. Inst. Meth. A **460**, 272 (2001).
[47] C. Mitsuda, T. Kajita, K. Miyano, S. Moriyama, M. Nakahata, Y. Takeuchi, and S. Tasaka, Nucl. Inst. Meth. A **497**, 414 (2003).
[48] J. O. Hirschfelder, C. F. Curtiss, and R. B. Bird, *Molecular Theory of Gases and Liquids* (Wiley, New York, 1954), p. 1110.
[49] V. P. Slyusar et al., Sov. J. Low. Temp. Phys. **4**, 363 (1978).
[50] J. J. van Loef, Physica B+C **103**, 362 (1981).